Electronic Supplementary Information

Ultrafine FeS_2 Nanocrystals/Porous Nitrogen-Doped Carbon Hybrid Nanospheres Encapsulated in Three-Dimensional Graphene for Simultaneously Efficient Lithium and Sodium Ion Storage

Zhonghui Chen,[ab] Shuo Li,[c] Yong Zhao,[a] Mohamed F. Aly Aboud,[d] Imran Shakir,[d,*] and Yuxi Xu[*b]

[a]Key Lab for Special Functional Materials of Ministry of Education, School of Materials Science and Engineering, Collaborative Innovation Center of Nano Functional Materials and Applications, Henan University, Kaifeng 475004, China.

[b]School of Engineering, Westlake University, 18 Shilongshan Road, Hangzhou 310024, Zhejiang Province, China.

[c]Department of Physical and Macromolecular Chemistry, Faculty of Science, Charles University, Hlavova 2030, Prague 2, Czech Republic.

[d]Sustainable Energy Technologies Center, College of Engineering, King Saud University, Riyadh 11421, Kingdom of Saudi Arabia

Material preparation

Synthesis of GO. GO was synthesized according to a modified Hummers' method. The graphite powder was in the size of 325 mesh and purchased from Aladdin Biochemical Technology Co., Ltd. All the other chemical reagents were purchased from Sinopharm Chemical Reagent Co., Ltd. and used without further purification.

Synthesis of Prussian Blue (PB) and PB/GO Aerogel. PB/GO was prepared by a modified excessive metal-ion-induced self-assembly route. Typically, uniformly dispersed GO solution (200 mL, 0.4 mg/mL) was first prepared. Then, $Na_4Fe(CN)_6$ solution (0.4 mL, 0.5 M) was added to it. After magnetic stirring for 30 min, $FeCl_3$ solution (4 mL, 0.5 M) was rapidly added to the above mixed solution. The mixed system was immediately turned blue. After aging for 1.5 h, the mixed solution was washed with deionized water for 3 times to remove the excess Fe^{3+}. Finally, the solid product after centrifugation was mixed with 2 mL of deionized water, and then freeze-dried into an aerogel (designated as PB/GO). Pure PB was synthesized in the same processes without the addition of GO.

Preparation of FeS_2/PNC@3DG and FeS_2/NC composites. The FeS_2/PNC@3DG composites were prepared by a facile one-step sulfidation strategy. Typically, the PB/GO aerogel was mixed with sulfur powder in a mass ratio of 1 : 5, and then put into a ceramic crucible which was sealed with aluminum foil. High purity nitrogen was injected into the tubular furnace to eliminate air. The mixed system was heated to 550 ^oC and maintained for 3 h to obtain FeS_2/PNC@3DG. The FeS_2/NC was prepared in the same process by replacing the PB/GO aerogel with PB.

Preparation of FeS_2. The FeS_2 was prepared by two conversion steps. First, PB was annealed at 350 ^oC in air for 2 h to obtain Fe_2O_3. In this step, the C and N elements in PB were removed, while Fe was oxidized to Fe_2O_3. Then, the Fe_2O_3 was sulfurated at 550 ^oC for 3 h to obtain pure FeS_2.

Preparation of PNC@3DG. The PNC@3DG was prepared by removing FeS_2 nanocrystals from the FeS_2/PNC@3DG aerogel. 5 mg of FeS_2/PNC@3DG aerogel was added into HCl solution (30 mL, 5 M), and then standing for 24 h. After centrifugation, the solid product was repeatedly washed with deionized water and freeze-dried to obtain the PNC@3DG. The microstructures of PNC@3DG were characterized to further demonstrate the nanostructures of the FeS_2/PNC@3DG.

Characterization

The microstructures and morphologies of the as-prepared samples were characterized on a field-emission scanning electron microscope (SEM, Zeiss Ultra-55) and high-resolution transmission electron microscopy (HRTEM, Nova NanoSem 450). X-ray diffraction (XRD) analysis from 10^o to 70^o was conducted on a D/Max 2500 X-ray diffractometer with Cu-Kα radiation (k=1.54 Å). Raman measurements were performed on an Invia/Reflrx Laser Micro-Raman spectroscope (Horiba Jobin Yvon, French). X-ray photoelectron spectroscopy (XPS) measurements were performed on a PHI 5000C ESCA System. Brunauer-Emmett-Teller (BET) tests were conducted on an Autosorb IQ Gas Sorption System at 77 K. Thermogravimetric analysis (TGA) was performed on a Mettler Toledo TGA instrument with the heating rate of 20 °C/min under 50 mL/min of flowing air.

Electrochemical measurements

The mechanically compressed FeS_2/PNC@3DG aerogel was directly used as anodes for LIBs and SIBs. The FeS_2, FeS_2/NC or PNC@3DG composites were mixed with poly(vinylidene fluoride) binder and Super P in a mass ratio of 8:1:1 to form a homogeneous slurry. The FeS_2/NC and PNC@3DG electrodes were prepared by coating the prepared slurry on Cu foil and dried in a vacuum oven at 100 ℃ for 12 h. All batteries were assembled in an argon-filled glovebox. LIBs were assembled with metallic lithium and Cellgard 2400 as the counter electrode and separator, respectively, and 1 M $LiPF_6$ in EC/DMC (1:1 by volume ratio) was used as the electrolyte. For SIBs, metallic sodium and glass fiber were used as the counter electrode and separator, respectively, and 1 M $NaClO_4$ in EC/DMC (1 : 1 by volume ratio) was used as the electrolyte.

The galvanostatic experiments of the assembled LIBs and SIBs were performed on a battery-testing system (LAND, Wuhan China) in the voltage window from 0.01 to 3 V. Electrochemical impedance spectroscopy (EIS) and Cyclic voltammetry (CV) measurements were conducted on a CHI 760D electrochemical workstation. EIS was measured in the frequency range of 0.01 Hz to 100 kHz. CV curves were measured in the potential range of 0.01−3 V at the scan rates from 0.1 to 2 mV s^{-1}.

Computational methods

All calculations were carried out at the density functional theory (DFT) level using the Vienna Ab initio Simulation Package (VASP). The Perdew–Burke–Ernzerhof (PBE) exchange–correlation functional was employed. The semi-empirical DFT-D3 method was used to treat the van der Waals interactions. An energy cut-off of 400 eV was used to determine the self-consistent charge density for the plane wave basis sets. The structures were fully optimized until the maximum Hellmann–Feynman force on atoms is less than 0.02 eV $Å^{-1}$ and the total energy variation is less than 1.0×10^{-5} eV. A vacuum of 15 Å was added in the perpendicular direction to the slab to model the isolated monolayers. Base on the experimental datas, we simulated several theoretical models, including FeS_2 (200), carbon nanosheet-FeS_2 (200), and N-doped carbon nanosheet-FeS_2 (200). The N-doped C-FeS_2 showed a N doping concentration of ~4.5%. Here, a 4×7×1 supercell of the square graphene contains 112 C atoms, and a 3×3×1 supercell of FeS_2 (200) contains 162 atoms including three layers of Fe atoms. Two layers of FeS_2 (200) are fixed as the slab model. The lattice mismatches between graphene and FeS_2 (200) are respectively 4.87% and 5.96 % along a and b axis. The adsorption energy (E_{ad}) is defined as $E_{ad} = E_{ion/substrate} - E_{ion} - E_{substrate}$, where $E_{ion/substrate}$, Eion, $E_{substrate}$ are the total energies of the substrate with the ion, the free ion, the corresponding substrate, respectively.

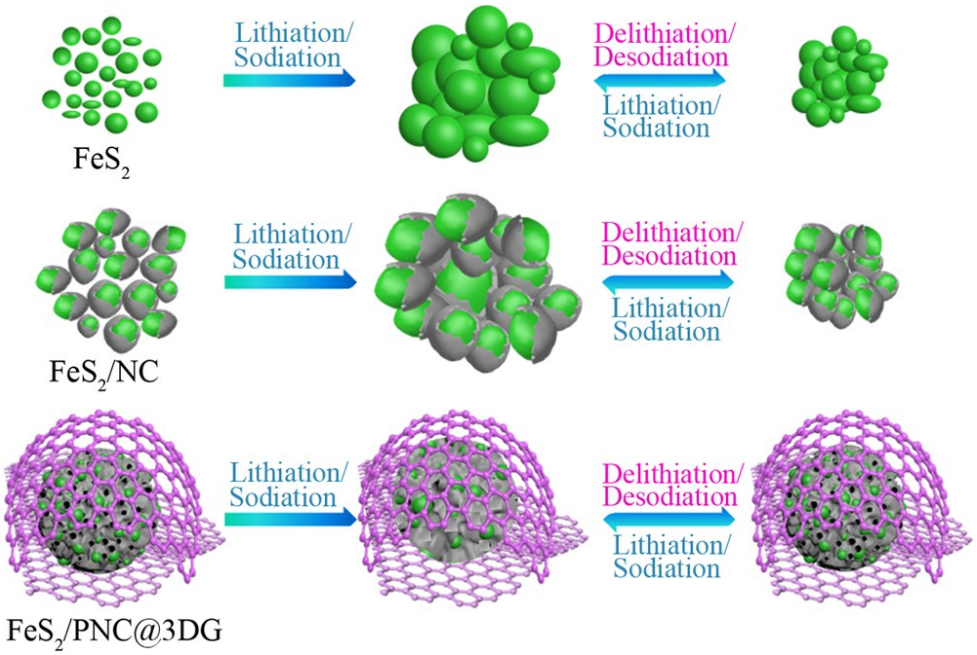

Scheme S1 Schematic illustration of the multistage protection mechanism of the FeS_2/PNC@3DG anode. In contrast, FeS_2 and FeS_2/NC anodes showed serious volume expansion and particle aggregation, which resulted in poor cycling stability and low electrochemical efficiency.

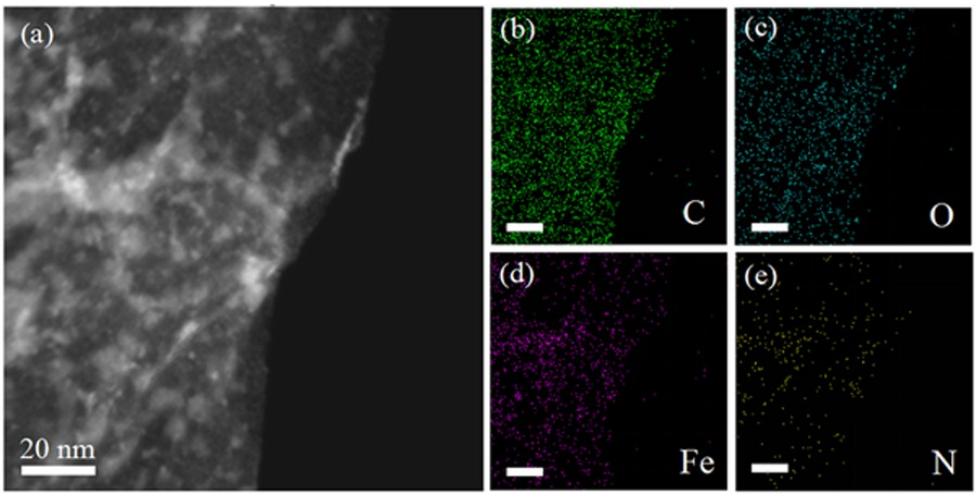

Fig. S1 (a) STEM image of the PB/GO precursor. (b-e) the corresponding elemental mappings of C, O, Fe and N. Scale bars, 50 nm.

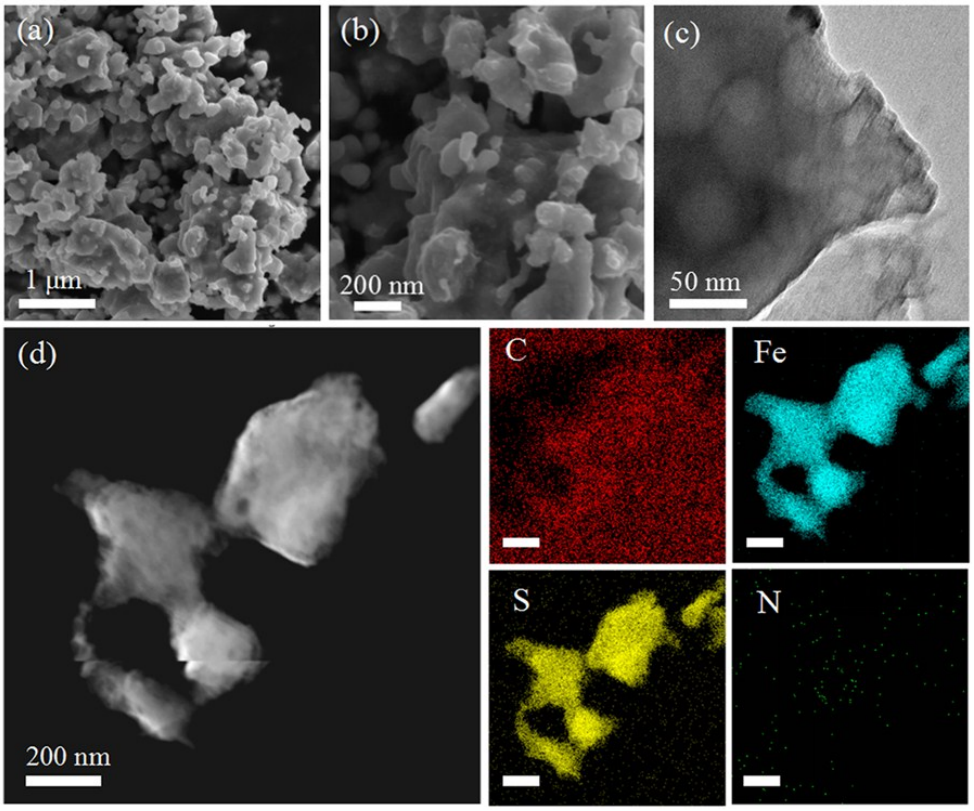

Fig. S2 The structural characterization of the FeS_2/NC (a,b) SEM, (c) TEM images. (d) STEM image and the corresponding elemental mappings of C, Fe, S and N.

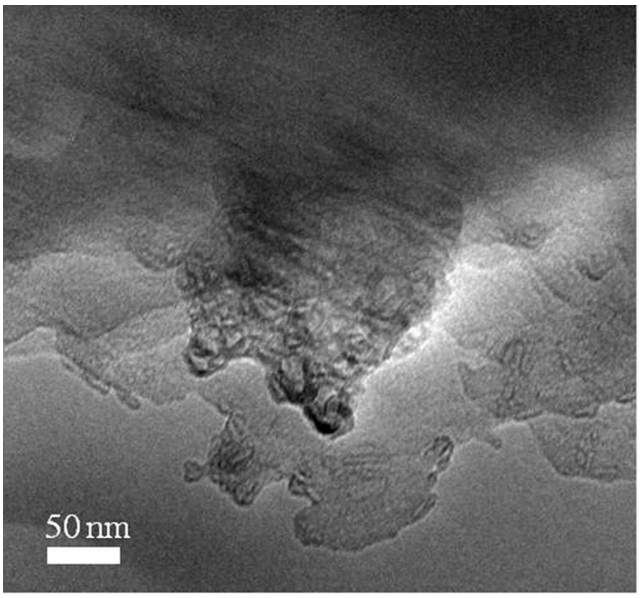

Fig. S3 (a,b) TEM images of the PNC@3DG.

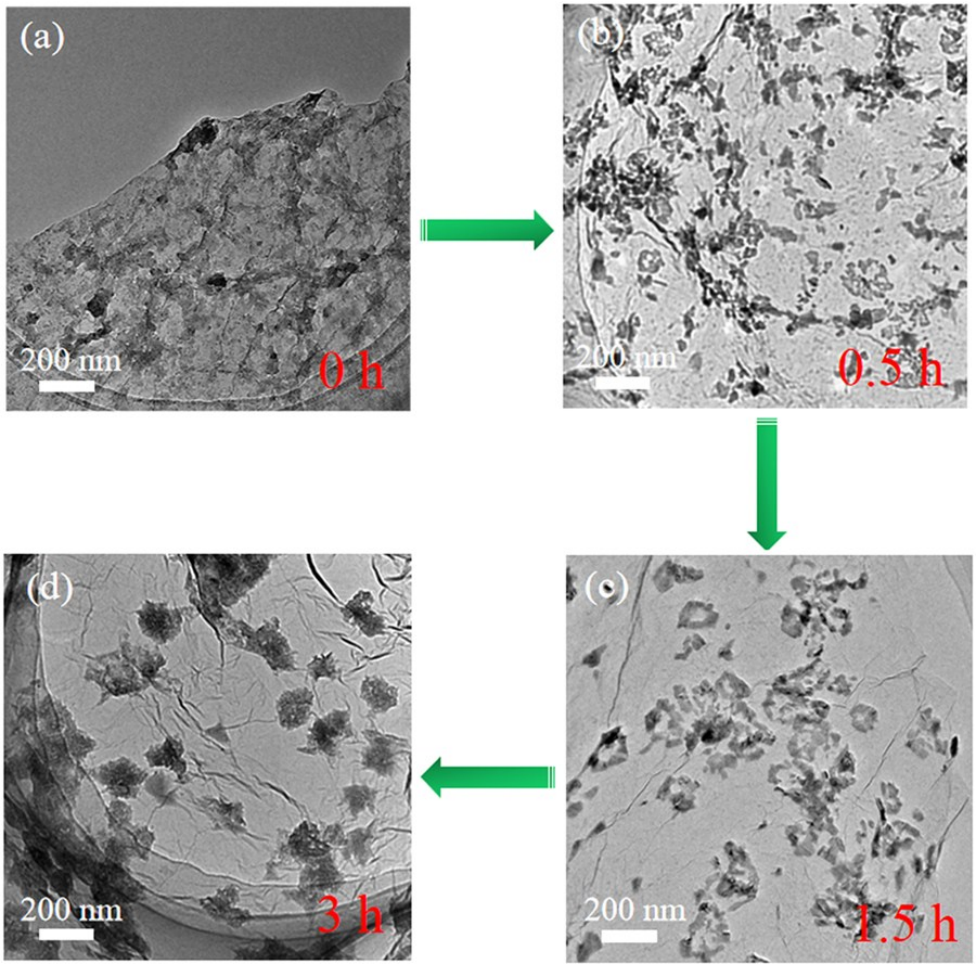

Fig. S4 The time-dependent structural evolution of the FeS_2/PNC@3DG composite. TEM images of the composites obtained by increasing temperature to 550 °C after (a) 0 h, (b) 0.5 h, (c) 1.5 h, (d) 3 h.

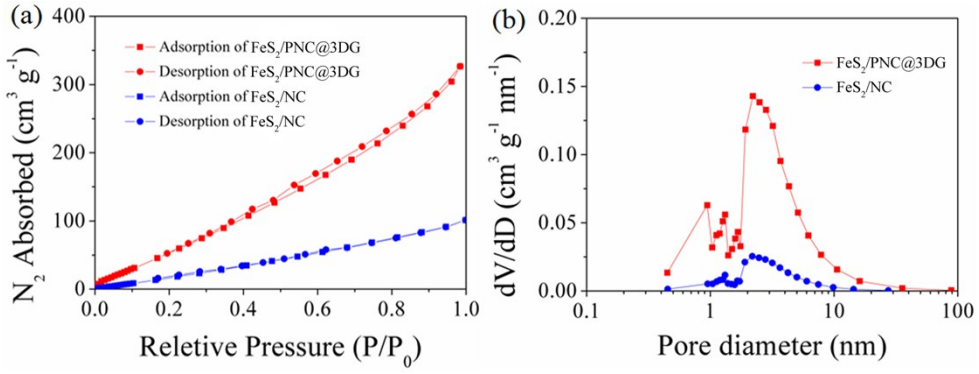

Fig. S5 (a) Nitrogen adsorption-desorption isotherms, (b) pore size distributions of the FeS_2/NC and FeS_2/PNC@3DG composites.

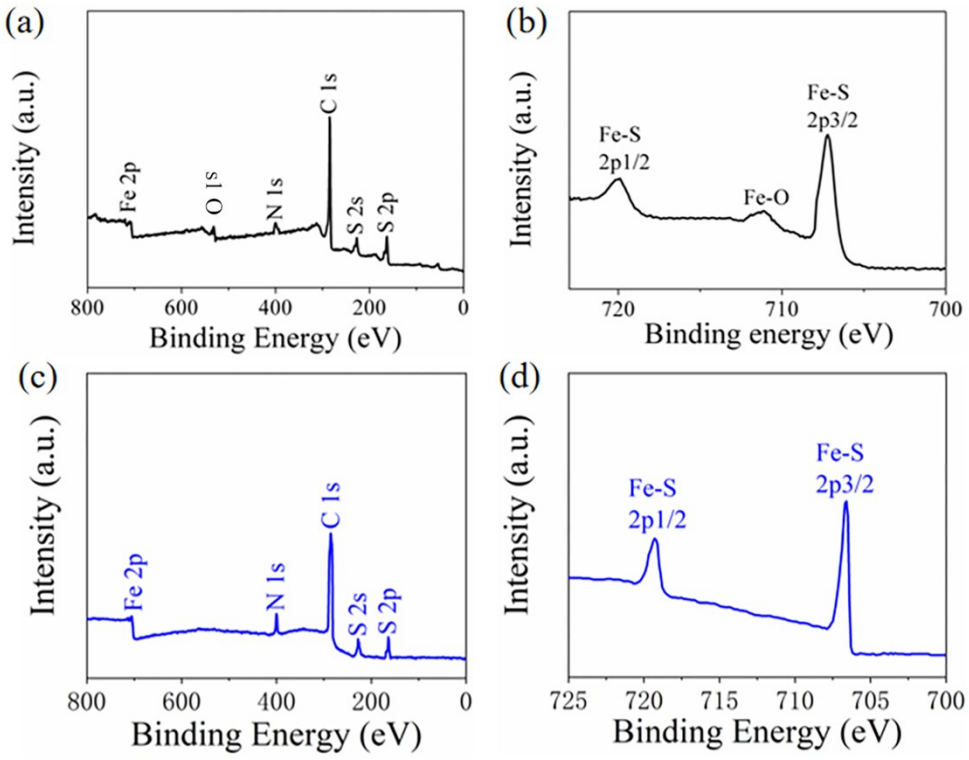

Fig. S6 (a) XPS survey spectrum, (b) Fe 2p spectrum of the FeS_2/PNC@3DG. (c) XPS survey spectrum, (b) Fe 2p spectrum of the FeS_2/NC.

Fig. S6a shows that C 1s, O1s, N 1s, Fe 2p, S 2s and S 2p peaks appear in the XPS survey spectrum of the FeS_2/PNC@3DG. The O elements come from the residual oxygen in 3DG and trace amounts of Fe-O bonds. The trace amounts of Fe-O bonds in Fig. S6b result from the reaction of Fe elements in PB and O elements in GO at the interface under high temperature. Two strong peaks at 707.2 and 720.1 eV in the Fe 2p spectrum (Fig. S6b) can be ascribed to Fe 2p1/2 and Fe 2p3/2 of FeS_2, which indicate the successful transformation of PB to FeS_2. In comparison, the FeS_2/NC consists of C, N, Fe and S elements without O (Fig. S6c). Its Fe 2p spectrum in Fig. S6d also demonstrates the successful transformation of PB to FeS_2.

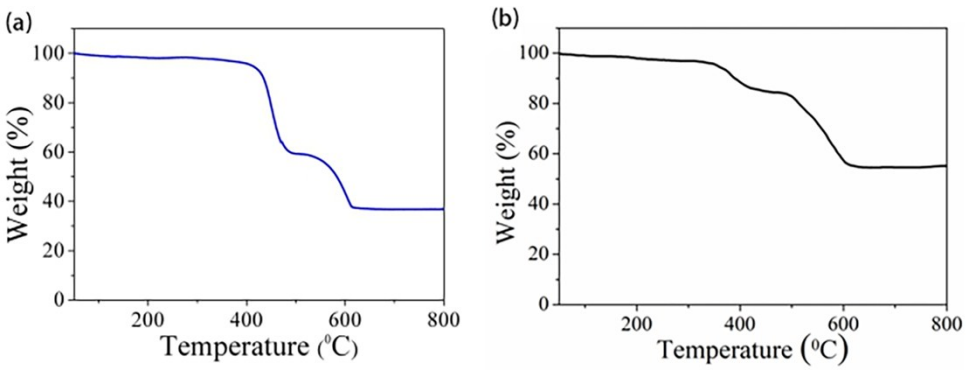

Fig. S7 TGA curves of (a) FeS_2/PNC@3DG and (b) FeS_2/NC composites at the heating rate of 20 °C/min under 50 mL/min of flowing air.

The FeS_2/PNC@3DG composite displays a minor weight loss of about 2% under 200 °C, which is due to the vapor of the residual water in the materials. The significant weight loss of about 61.2% between 400 and 600 °C is caused by the phase change of FeS_2 to Fe_2O_3 and rGO to carbon dioxide. The final residual sample is Fe_2O_3, and its weight ratio is 36.8%. As a result, the weight content of FeS_2 in the FeS_2/PNC@3DG is calculated to be 55.2%. After deducting the residual water in the materials (~2%), the actual weight content of FeS_2 is 56.3%. Through the same calculation method, the weight ratio of FeS_2 in the FeS_2/NC was calculated to be 84.1%.

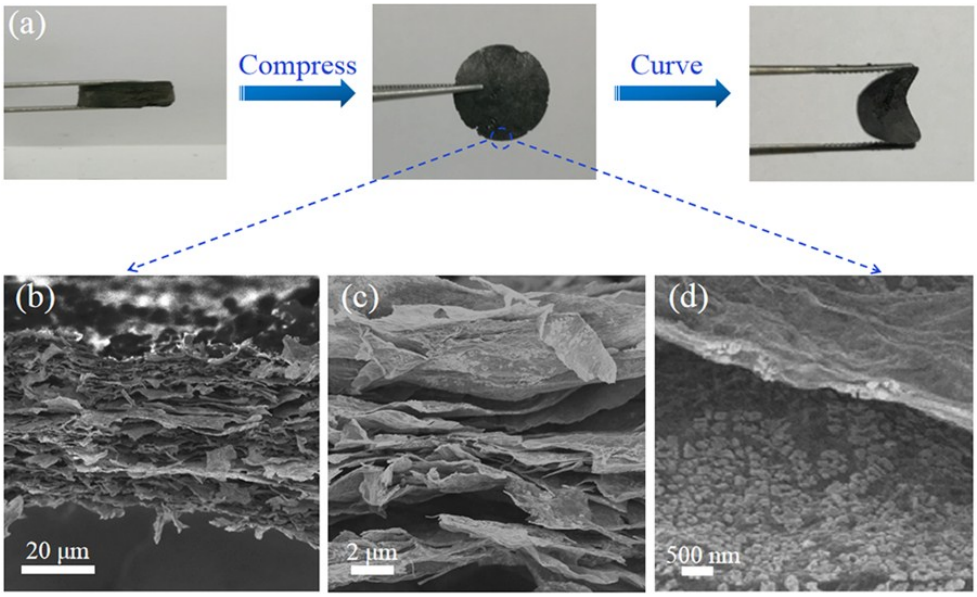

Fig. S8 (a) Preparation of a flexible binder-free FeS_2/PNC@3DG anode, (b-d) SEM images of the side-view of the pressed FeS_2/PNC@3DG film under different magnifications.

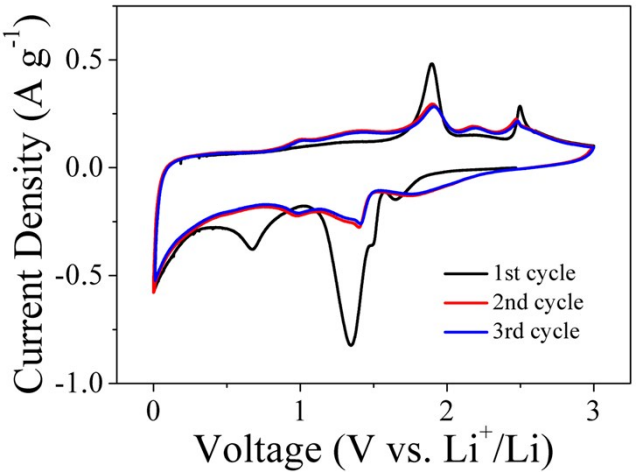

Fig. S9 CV curves for the initial three cycles of the FeS_2/PNC@3DG anode at 0.1 mV s^{-1} for LIBs.

There are two peaks at 1.35 and 0.67 V in the first cathodic scan, which can be ascribed to the insertion of Li^+ into FeS_2 nanocrystals ($FeS_2+4Li^++4e^-\rightarrow Fe+2Li_2S$) and the formation of a solid electrolyte interlayer (SEI) film, respectively. In the first anode scan, the peak at 1.89 V can be ascribed to the formation of $Li_{2-x}FeS_2$ related to the two reactions ($Fe+2Li_2S\rightarrow Li_2FeS_2+2Li^++2e^-$ and $Li_2FeS_2\rightarrow Li_{2-x}FeS_2+xLi^++xe^-$), and the peak at 2.5 V is associated with the generation of FeS_y and S. It is worth noting that two reduction peaks at 2.02 and 1.41 V appear in the subsequent two cycles, corresponding to the two reactions: $FeS_y+(2-y)S+2Li^++2e^-\leftrightarrow Li_2FeS_2$ and $Li_2FeS_2+2Li^++2e^-\leftrightarrow Fe+2Li_2S$, respectively.

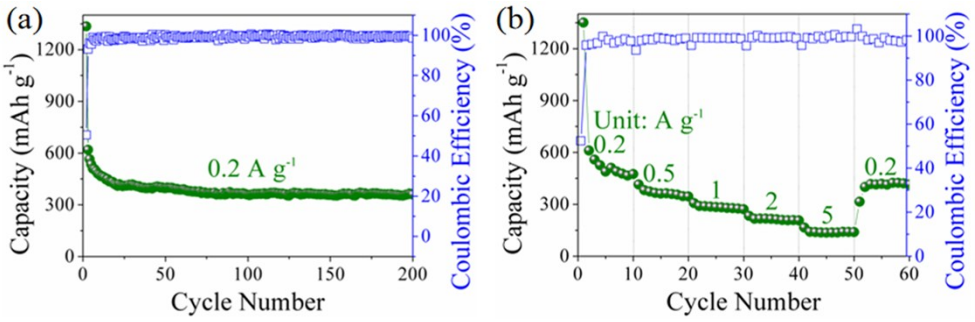

Fig. S10 (a) Cycling performance at 0.2 A g^{-1} for 200 cycles, (b) Rate performance of the PNC@3DG anode for LIBs.

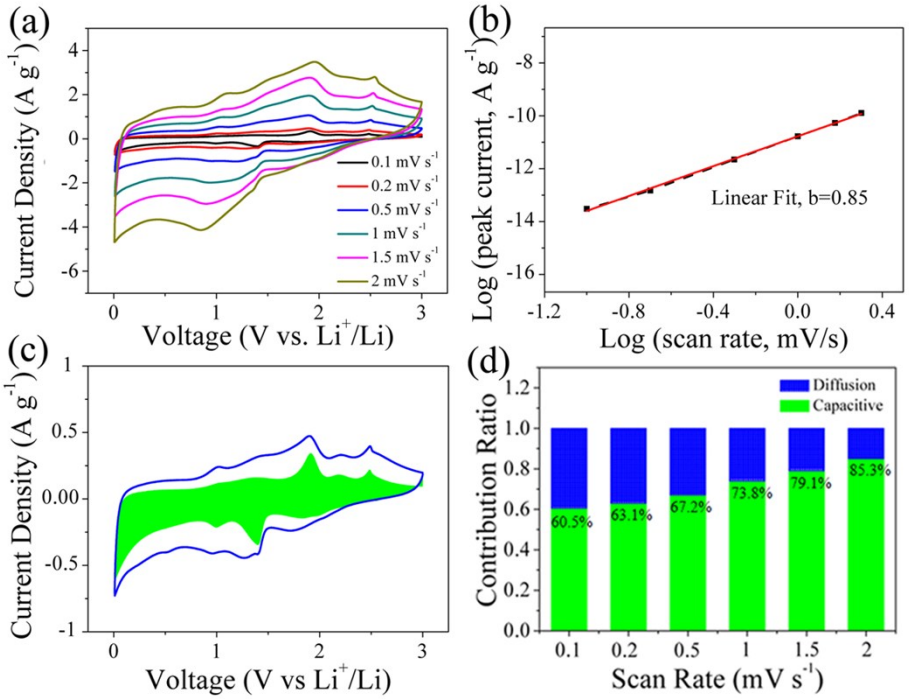

Fig. S11 The kinetic analysis of the FeS_2/PNC@3DG anodes for LIBs. (a) CV curves at different scan rates from 0.1 to 2 mV s^{-1}. (b) The b value calculated from peak currents and scan rates from (a). (c) CV curves with the capacitive contribution (green section) to the total current at 0.1 mV s^{-1}. (d) Contribution ratios of the capacitive and diffusion-controlled capacities at different scan rates.

With a 20-fold increment in scan rates, the CV curves of the FeS_2/PNC@3DG anodes still exhibit a similar shape, as shown in Fig. S11a. The reaction kinetics were further analyzed based on the equation of $i = av^b$, where i was the peak current, ν was the sweep rate, a and b were empirical parameters. The b value close to 0.5 represents a diffusion controlled behavior, whereas the value of 1 suggests an ideal capacitive behavior. The calculated b value of the FeS_2/PNC@3DG anode was 0.85 (Fig. S11b), indicating its fast reaction kinetics originate from the pseudocapacitive effect. Furthermore, the diffusion-controlled and capacitive-controlled fractions can be distinguished according to the equation of $i = k_1\nu_{1/2} + k_2\nu$, where k_1 and k_2 can be calculated by plotting $i/\nu_{1/2}$ vs $\nu_{1/2}$. The capacitive current ($i_2 = k_2\nu$) can be extracted from the total current, as shown in Fig. S12c. The capacitive-controlled fraction of the FeS2/PNC@3DG anode at 0.1 mV s^{-1} was calculated to be 60.5%. In addition, based on the same method, all capacitive-controlled fractions at different sweep rates (0.2, 0.5, 1, 1.5, 2 mV s^{-1}) were determined to be 63.1%, 67.2%, 73.8%, 79.1% and 85.3%, respectively, as shown in Fig. S12d.

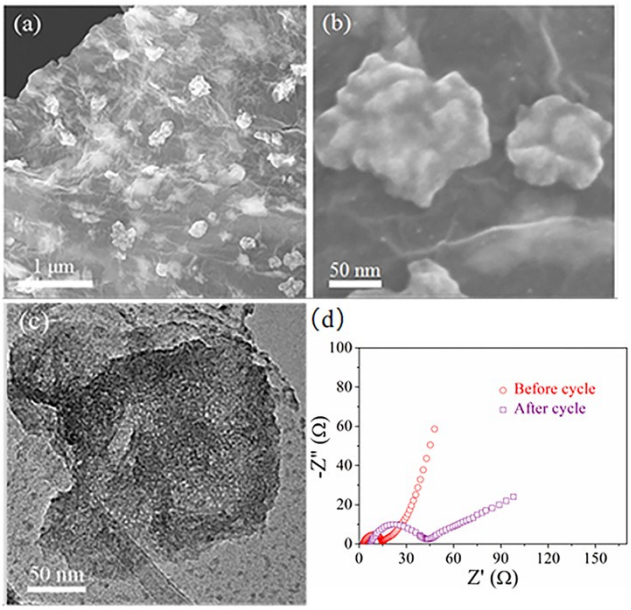

Fig. S12 (a,b) SEM images, (c) TEM images of the FeS_2/PNC@3DG anode for LIBs after long cycling tests. (d) EIS plots of FeS_2/PNC@3DG anodes for LIBs before and after long cycling tests.

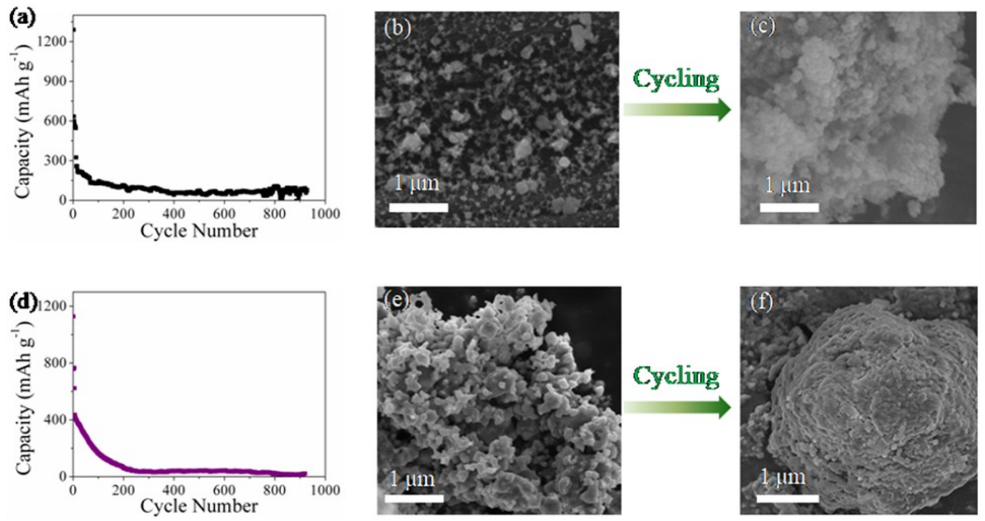

Fig. S13 (a) Cycle performance of the FeS_2 anode at 5 A g^{-1}, SEM images of the FeS_2 anode before (b) and after (c) cycling tests. (d) Cycle performance of the FeS_2/NC anode at 5 A g^{-1}, SEM images of the FeS_2/NC anode before (e) and after (f) cycling tests.

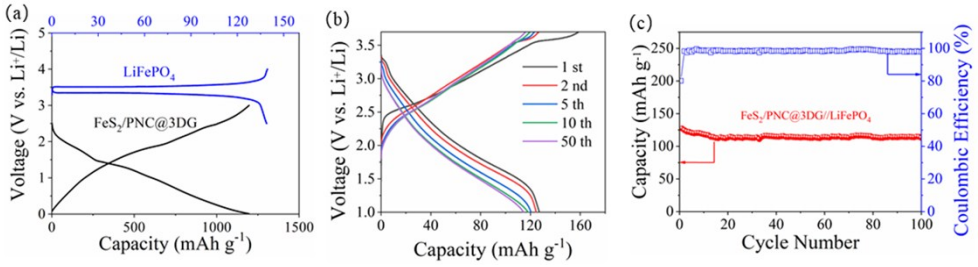

Fig. S14 Electrochemical performance of the FeS_2/PNC@3DG//$LiFePO_4$ full cell. (a) Charge-discharge voltage profiles of the single electrodes: FeS_2/PNC@3DG anode (down curve) at 200 mA g^{-1} and the $LiFePO_4$ cathode (up curve) at 100 mA g^{-1} versus Li. (b) Charge-discharge voltage profiles at 100 mA g^{-1}, (c) Cycling performance of the FeS_2/PNC@3DG//$LiFePO_4$ full cell at 100 mA g^{-1}.

The FeS_2/PNC@3DG//$LiFePO_4$ full cell was prepared by following procedures. The $LiFePO_4$ cathode was prepared by mixing 10 wt% Super-P, 10 wt% PVDF and 80% $LiFePO_4$, dissolved in NMP to form a slurry, which was then pasted on Al foil. The FeS_2/PNC@3DG anodes were precycled in half-cells and then assembled into full cells. The cathode capacity was limited, and the cathode-to-anode specific capacity loading ratio was 1:1.1. The $LiFePO_4$ cathode exhibited a reversible capacity of ~139 mA h g^{-1} and a flat voltage plateau of ~3.5 V. On the basis of the results from half-cells, the voltage window of the full cell was set as 2.2-3.7 V.

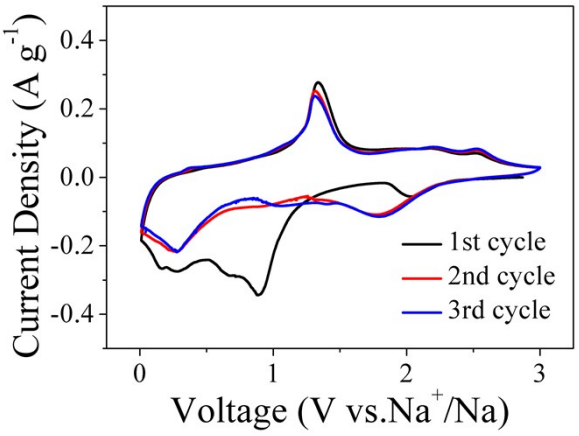

Fig. S15 CV curves for the initial three cycles of the FeS_2/PNC@3DG anode at 0.1 mV s^{-1} for SIBs.

During the first cathodic scan, the larger peak at 0.91 V corresponds to the insertion of Na^+ into FeS_2 nanocrystals to form $Na_{2-x}FeS_2$, and a broad reduction peak near 0.28 V results from the subsequent conversion to produce Na_2S and highly reactive nano-Fe^0 as well as the formation of SEI films. For the anodic scan, three peaks at 1.32, 2.21 and 2.53 V appears, which can be ascribed to the multi-step reaction mechanism for desodiation procedures and the final formation of $Na_{2-x}FeS_2$ species. For the subsequent two cycles, its cathodic/anodic peaks are coincident with the reversible reactions between nano-Fe^0, Na_2S and Na_2FeS_2.

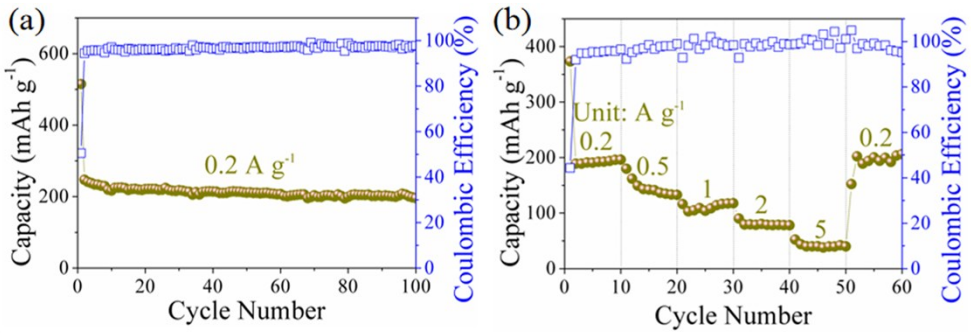

Fig. S16 (a) Cycling performance at 0.2 A g^{-1} for 200 cycles, (b) Rate performance of the PNC@3DG anode for SIBs.

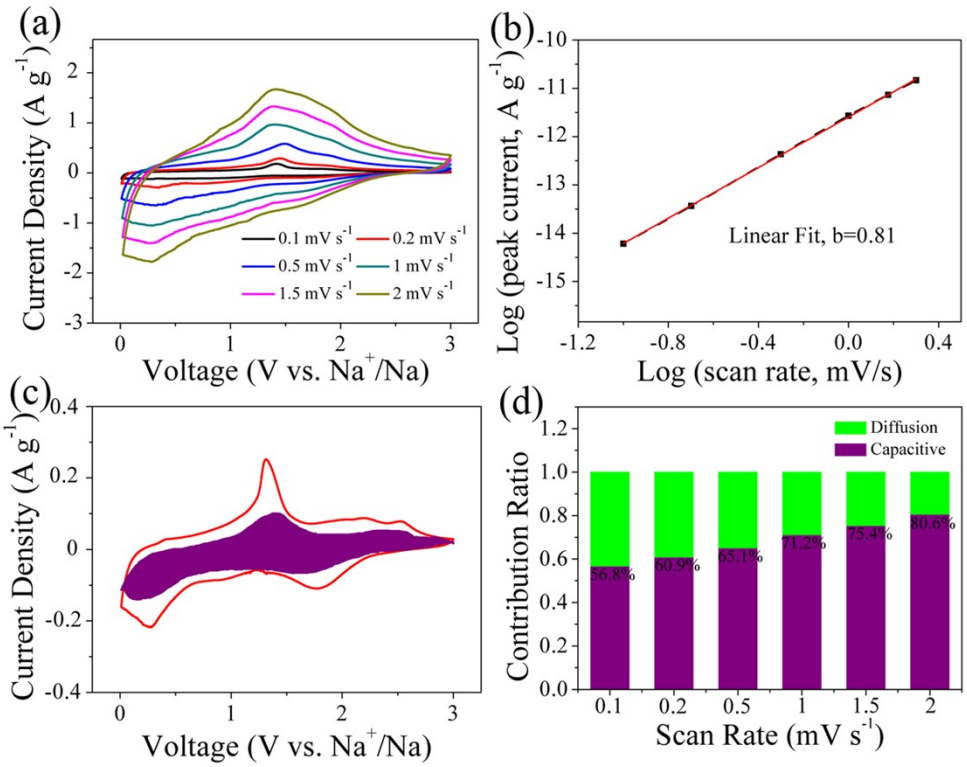

Fig. S17 The kinetic analysis of the FeS_2/PNC@3DG anodes for SIBs. (a) CV curves at different scan rates from 0.1 to 2 mV s^{-1}. (b) The b value calculated from peak currents and scan rates from (a). (c) CV curves with the capacitive contribution (green section) to the total current at 0.1 mV s^{-1}. (d) Contribution ratios of the capacitive and diffusion-controlled capacities at different scan rates.

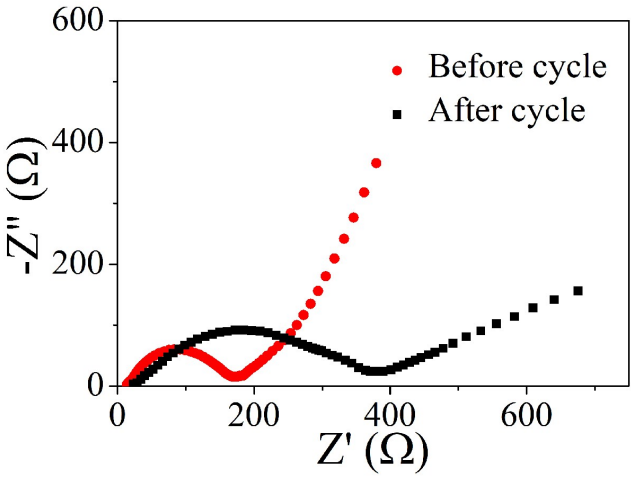

Fig. S18 EIS plots of FeS_2/PNC@3DG anodes for SIBs before and after long cycling tests.

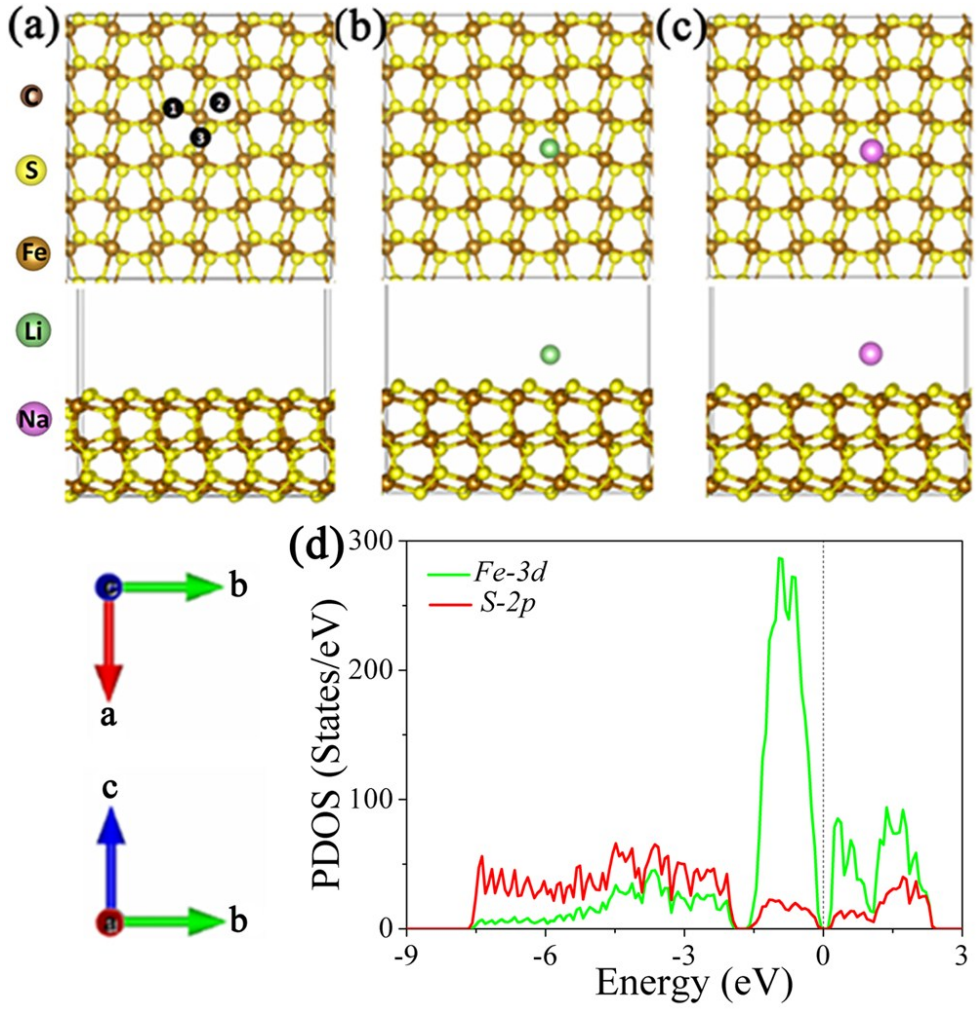

Fig. S19 Top view and side view of (a) FeS_2 (200) configuration, (b) Li adsorption on FeS_2 (200), (c) Na adsorption on FeS_2 (200). The spheres with different colors denoted C, N, S, Fe, Li and Na atoms, respectively. (d) Projected density of states of FeS_2.

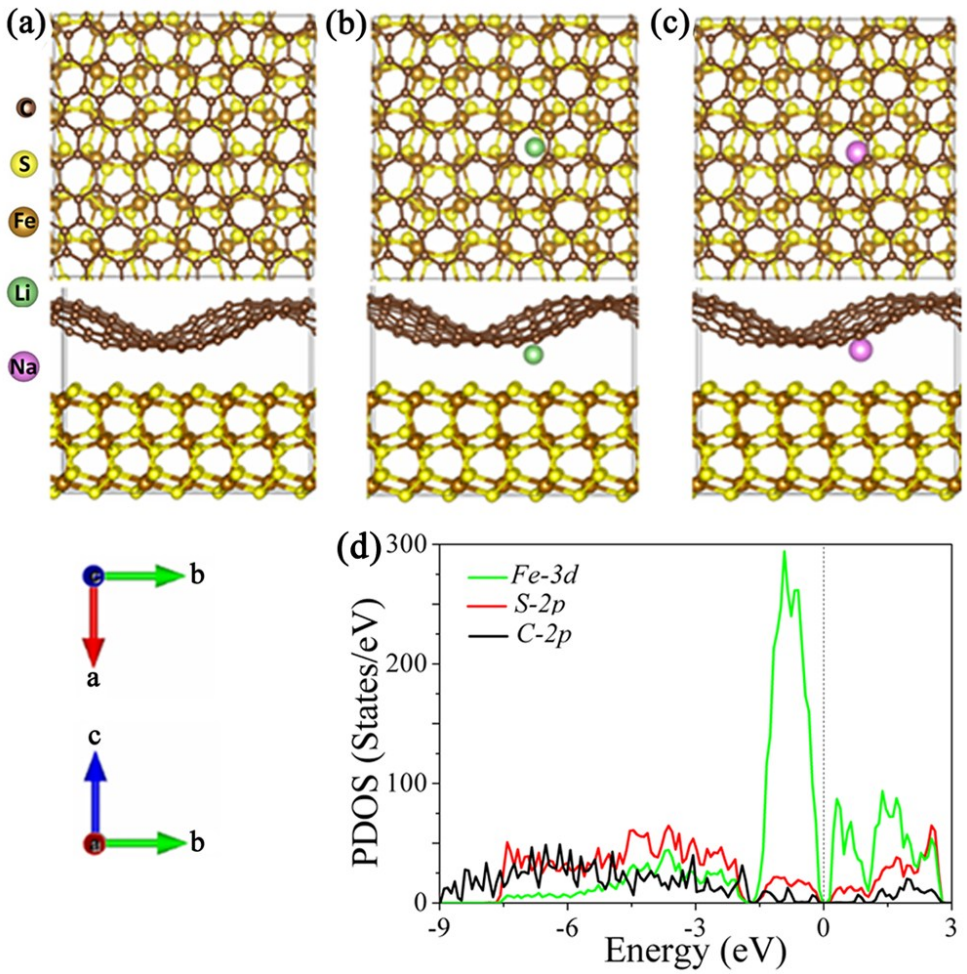

Fig. S20 Top view and side view of (a) C-FeS_2 (200) configuration, (b) Li adsorption on C-FeS_2 (200), (c) Na adsorption on C-FeS_2 (200). The spheres with different colors denoted C, N, S, Fe, Li and Na atoms, respectively. (d) Projected density of states of C-FeS_2.

Table S1. Comparison of the electrochemical performance of the FeS_2/PNC@3DG with previously reported metal sulfide based LIBs.

Materials	Ratio of active materials	Current density	Capacity (mAh g^{-1}) / after cycles	High current density	Capacity (mAh g^{-1}) / after cycles	Capacity Retention (Long Cycles)	Ref.
FeS_2@C	80%	0.1 A g^{-1}	720/10 576 **(by electrode)**	10 A g^{-1}	400/10 320 **(by electrode)**	~90% (120)	*ACS Nano 2017, 11, 9033*
FeS_2@C porous nanooctahedra	85%	0.45 A g^{-1}	500/50 425 **(by electrode)**	4.5 A g^{-1}	256/5 217.6 **(by electrode)**	N.A.	*Adv. Mater. 2014, 26, 6025*
PAN-FeS_2	60%	0.1 C	470/50 282 **(by electrode)**	N.A.	N.A.	N.A.	*Adv. Energy Mater. 2014, 4, 1300961*
FeS_2 /rGO	80%	0.18 A g^{-1}	1202/5 961.6 **(by electrode)**	17.8 A g^{-1}	237/5 189.6 **(by electrode)**	68% (2000)	*J. Mater. Chem. A 2015, 3, 7945*
FeS_2/N-G	80%	0.1 C	849/100 679.2 **(by electrode)**	1 C	762/10 609.6 **(by electrode)**	N.A.	*Electrochim. Acta 2014, 137, 197*
FeS_2-GNS -CNT	80%	0.25 A g^{-1}	850/100 680 **(by electrode)**	8 A g^{-1}	330/10 264 **(by electrode)**	95.6% (350)	*J. Power Sources 2017, 342, 105*
FeS_2@ porous C	76%	0.2 C	860/10 653.6 **(by electrode)**	2 C	720/10 547.2 **(by electrode)**	N.A.	*J. Power Sources 2016, 331, 366*
3DGF-FeS_2	100%	0.2 A g^{-1}	1080.3/100 **(by electrode)**	5 A g^{-1}	350/10 **(by electrode)**	N.A.	*Carbon 2017, 114, 111*
NiS_2@CoS_2 @C@C nanocubes	70%	0.1 A g^{-1}	1160/5 812 **(by electrode)**	5 A g^{-1}	415/5 290 **(by electrode)**	N.A.	*Energy Storage Mater. 2018, 11, 67*
CoS_2 nanobubble hollow prisms	70%	0.2 A g^{-1}	910/10 637 **(by electrode)**	5 A g^{-1}	470/10 329 **(by electrode)**	85% (200)	*Angew. Chem. Int. Ed. 2016, 55, 13422*
WS_2/rGO	80%	0.1 A g^{-1}	953.1/100 762.5 **(by electrode)**	5 A g^{-1}	620/10 496 **(by electrode)**	86.1% (350)	*Carbon 2019, 142, 697*
CuS nanorods	70%	0.056 A g^{-1}	400/10 280 **(by electrode)**	2.8 A g^{-1}	182/10 127.4 **(by electrode)**	~97% (250)	*J. Power Sources 2016, 306, 408*
CNF@NiS	100%	0.1	1152/10	3 A g^{-1}	664.3	~82%	*Adv. Mater. Interfaces*

		A g^{-1}	**(by electrode)**		**(by electrode)**	(100)	*2016, 3, 1500467*
FeS_2/PNC @3DG	**100%**	**0.2 A g^{-1}**	**1208/200 (by electrode)**	**5 A g^{-1}**	**829/10 (by electrode)**	**94.2% (1000)**	**This work**

Note: In typical electrode preparation reported previously, polymer binders and conductive carbon were used to mix with active materials to prepare electrodes. It is more meaningful to normalize the capacity to the total mass of the entire electrode for practical application. Therefore, we specially list these capacity values (denoted as "by electrode") for comparison.

Table S2. Comparison of the electrochemical performance of the FeS_2/PNC@3DG with previously reported metal sulfide based SIBs.

Materials	Ratio of active materials	Current density	Capacity (mAh g^{-1}) / after cycles	High current density	Capacity (mAh g^{-1}) / after cycles	Capacity Retention (Long Cycles)	Ref.
FeS_2@C	70%	0.1 A g^{-1}	511/100 357.7 **(by electrode)**	5 A g^{-1}	403/10 282.1 **(by electrode)**	~70% (800)	*Energy Environ. Sci., 2017, 10, 1576*
FeS_2/CNT	80%	0.2 A g^{-1}	394/400 315.2 **(by electrode)**	22 A g^{-1}	~300/10 240 **(by electrode)**	~70% (8400)	*Nano Energy 2018, 46, 117*
FeS_2@rGO	80%	0.2 C	315.6/5 252.5 **(by electrode)**	2 C	192.9/5 154.3 **(by electrode)**	79.2% (250)	*Electrochim. Acta 2017, 230,1*
FeS_2/rGO aerogel	80%	0.18 A g^{-1}	267/200 213.6 **(by electrode)**	4.5 A g^{-1}	195/5 156 **(by electrode)**	58% (800)	*J. Mater. Chem. A, 2017, 5, 5332*
FeS-rGO	70%	0.5 A g^{-1}	547/50 382.9 **(by electrode)**	6 A g^{-1}	340/10 238 **(by electrode)**	N.A.	*Chem. Eur. J. 2016, 22, 2769*
Co-Doped FeS_2 nanospheres	80%	0.05 A g^{-1}	400/5 320 **(by electrode)**	20 A g^{-1}	173/5 138.4 **(by electrode)**	~75% (400)	*Angew. Chem. Int. Ed. 2016, 55, 12822*
$Fe_{1-x}S$@ CNTs	80%	0.2 A g^{-1}	492.7/10 394.2 **(by electrode)**	8 A g^{-1}	326.3/10 261 **(by electrode)**	~67.4% (300)	*ACS Energy Lett. 2017, 2, 364*
$Fe_{1-x}S$@ PNCNWs /rGO	100%	0.2 A g^{-1}	565/10 **(by electrode)**	5 A g^{-1}	240/10 **(by electrode)**	~50% (200)	*Adv. Energy Mater. 2019, 1803052*
CoS@C nanowires	90%	0.1 A g^{-1}	379/5	5 A g^{-1}	235/5	84% (200)	*Adv. Mater. 2016, 28,*

			341 **(by electrode)**		211.5 **(by electrode)**		*7276*
CoS_2-CoS-GC	70%	0.1 A g^{-1}	530/10 371 **(by electrode)**	1 A g^{-1}	411/10 287.7 **(by electrode)**	69% (100)	*Nano Energy 2016, 26, 466.*
Hollow NiS spheres	70%	0.2 A g^{-1}	511.5/4 358 **(by electrode)**	5 A g^{-1}	337.4/4 236 **(by electrode)**	73% (50)	*Adv. Funct. Mater. 2016, 26, 7479*
NiS_2/NC	80%	0.1 A g^{-1}	505.7/100 404.6 **(by electrode)**	3 A g^{-1}	294.4/10 235.5 **(by electrode)**	69% (300)	*J. Mater. Chem. A, 2018, 6, 6595*
WS_2/rGO Nano-HC	80%	0.1 A g^{-1}	522.3/70 417.8 **(by electrode)**	5 A g^{-1}	75/10 60 **(by electrode)**	66.1% (200)	*Carbon 2019, 142,697*
FeS_2/PNC @3DG	**100%**	**0.2 A g^{-1}**	**597/100 (by electrode)**	**5 A g^{-1}**	**316/10 (by electrode)**	**85.2% (800)**	**This work**

Table S3. The adsorption energies (E_{ad}) of Li and Na adsorption on FeS_2 (200), (b) C-FeS_2 (200) and (c) NC-FeS_2 (200).

Compounds	E_{ad}	
	Li	Na
FeS_2	-2.39	-1.98
C-FeS_2	-2.72	-2.37
NC-FeS_2	-2.80	-2.42